A model of the Arctic Ocean carbon cycle

M. Manizza,[1,2] M. J. Follows,[1] S. Dutkiewicz,[1] D. Menemenlis,[3] J. W. McClelland,[4] C. N. Hill,[1] B. J. Peterson,[5] and R. M. Key[6]

Received 27 January 2011; revised 19 September 2011; accepted 30 September 2011; published 15 December 2011.

[1] A three dimensional model of Arctic Ocean circulation and mixing, with a horizontal resolution of 18 km, is overlain by a biogeochemical model resolving the physical, chemical and biological transport and transformations of phosphorus, alkalinity, oxygen and carbon, including the air-sea exchange of dissolved gases and the riverine delivery of dissolved organic carbon. The model qualitatively captures the observed regional and seasonal trends in surface ocean PO_4, dissolved inorganic carbon, total alkalinity, and pCO_2. Integrated annually, over the basin, the model suggests a net annual uptake of 59 Tg C a^{-1}, within the range of published estimates based on the extrapolation of local observations (20–199 Tg C a^{-1}). This flux is attributable to the cooling (increasing solubility) of waters moving into the basin, mainly from the subpolar North Atlantic. The air-sea flux is regulated seasonally and regionally by sea-ice cover, which modulates both air-sea gas transfer and the photosynthetic production of organic matter, and by the delivery of riverine dissolved organic carbon (RDOC), which drive the regional contrasts in pCO_2 between Eurasian and North American coastal waters. Integrated over the basin, the delivery and remineralization of RDOC reduces the net oceanic CO_2 uptake by ∼10%.

Citation: Manizza, M., M. J. Follows, S. Dutkiewicz, D. Menemenlis, J. W. McClelland, C. N. Hill, B. J. Peterson, and R. M. Key (2011), A model of the Arctic Ocean carbon cycle, *J. Geophys. Res.*, *116*, C12020, doi:10.1029/2011JC006998.

1. Introduction

[2] The Arctic Ocean is a unique basin, sitting at the pole and enclosed by large continental land masses. It provides a conduit for the exchange of waters and their biogeochemical properties between the Pacific and Atlantic basins. The cold, high latitude situation of the Arctic basin suggests that it should be a regional sink of atmospheric carbon dioxide in the "natural" carbon cycle, and also a sink for anthropogenic carbon. Air-sea fluxes of carbon in the Arctic Ocean may be driven by the large-scale transport of dissolved inorganic carbon (DIC) into and out of the basin, biological production and respiration of organic carbon, regional and seasonal patterns of temperature (and solubility) variation, as well as the respiration of RDOC to DIC. Extrapolation of still relatively (regionally and seasonally) sparse observations of surface pCO_2 suggest a net annual uptake of carbon dioxide by the Arctic Ocean somewhere between 20 and 200 Tg C a^{-1} (1 Tg = 10^{12} g) [*Bates*, 2006; *Bates and Mathis*, 2009; *McGuire et al.*, 2009]. Here we describe a model of Arctic Ocean circulation and biogeochemistry with which we simulate the regional carbon cycle, comparing the simulation with observed distributions of key biogeochemical tracers, estimating regional and seasonal air-sea fluxes of CO_2, and identifying the forcing from different processes.

[3] We also focus on evaluating the role of riverine delivery of dissolved organic carbon to the Arctic Ocean. Mediated by rivers, the terrestrial ecosystems of the surrounding land masses supply between 35 and 40 Tg C annually [*Raymond et al.*, 2007; *Batjes*, 1997] to the Arctic Ocean where a fraction is converted into inorganic carbon both by heterotrophic respiration of microbes and by photo-oxidation [*Amon and Meon*, 2004; *Bélanger et al.*, 2006]. Observed salinity-DOC relationships suggest that this occurs with an e-folding timescale of about 10 years [*Hansell et al.*, 2004; *Cooper et al.*, 2005], with some of the RDOC transported out of the basin before respiration. In contrast to the large, open ocean basins, terrigenous DOC could be an important factor in regulating the basin-wide air-sea exchange in the Arctic. Here we use a circulation and biogeochemistry model to explore its local and integrated impact in the basin. The manuscript is organized in the following way: In section 2, we describe the ocean circulation and biogeochemistry model. In section 3, we discuss model solutions, considering the simulation of regional carbon cycle characteristics and exploring the sensitivity of the air-sea CO_2 fluxes to source

[1]Department of Earth, Atmospheric and Planetary Sciences, Massachusetts Institute of Technology, Cambridge, Massachusetts, USA.
[2]Now at Geosciences Research Division, Scripps Institution of Oceanography, University of California, San Diego, La Jolla, California, USA.
[3]Jet Propulsion Laboratory, California Institute of Technology, Pasadena, California, USA.
[4]Marine Science Institute, University of Texas at Austin, Port Aransas, Texas, USA.
[5]Ecosystems Center, Marine Biological Laboratory, Woods Hole, Massachusetts, USA.
[6]Department of Geosciences, Princeton University, Princeton, New Jersey, USA.

0148-0227/11/2011JC006998

and remineralization of RDOC. In section 4, we summarize and discuss the model results in a broader context.

2. Model Description

2.1. Regional Arctic Ocean Model

[4] The regional Arctic modeling framework which we develop and apply here was previously used to study the freshwater budget [*Condron et al.*, 2009] and the transport of RDOC [*Manizza et al.*, 2009] in the Arctic basin. Here we extend the framework to include explicit, but idealized, representations of physical, chemical and biological processes that regulate regional carbon and nutrient cycles. At the heart of the model are simulations of ocean circulation using the MIT General Circulation Model (MITgcm) [*Marshall et al.*, 1997] with a coupled sea-ice model. The model is configured on a "cubed-sphere" grid in a limited area Arctic domain with open boundaries at ≈55°N in the Atlantic and Pacific sectors. Prescribed boundary conditions for potential temperature, salinity, flow and sea-surface elevation are provided from previous integrations of a global configuration of the same model [*Menemenlis et al.*, 2005]. The grid is locally orthogonal and has a variable horizontal resolution with an average spacing of ∼18 km. The mesh resolves major Arctic straits, including many of the channels of the Canadian Archipelago. The sea-ice and fluid dynamical equations are solved on the same horizontal mesh. The vertical grid is height based, varying from 10 m thick near the surface to ∼450 m at a depth of ∼6 km in 50 levels. Bathymetry is derived from the U.S National Geophysical Data Center (NGDC) two-minute global relief data set (ETOPO2), which uses the International Bathymetric Chart of the Arctic Ocean (IBCAO) product for Arctic bathymetry [*Jakobsson et al.*, 2008]. The ETOPO2 data is smoothed to the model horizontal mesh and mapped to the ocean vertical levels using a "lopped cell" strategy [*Adcroft et al.*, 1997], which permits accurate representation of the ocean bottom boundary.

[5] The ocean model's hydrography is initialized with observations taken from the Polar Science Center Hydrographic Climatology (PHC) 3.0 database [*Steele et al.*, 2001]. Initial sea-ice distributions are taken from the Pan-Arctic Ice-Ocean Modeling and Assimilation System data sets [*Zhang and Rothrock*, 2003]. Atmospheric state (10-m surface winds, 2-m air temperatures and humidities and downward long and short-wave radiation) is taken from the six-hourly data sets of the National Centers for Environmental Prediction reanalysis [*Kalnay et al.*, 1996]. Monthly mean estuarine fluxes of fresh water are based on the Arctic Runoff database [*Lammers et al.*, 2001; *Shiklomanov et al.*, 2000]. The sea-ice component of the coupled system follows the viscous-plastic rheology formulation of *Hibler* [1979] with momentum equations solved implicitly on a C-grid [*Arakawa and Lamb*, 1977] using a procedure based on *Zhang and Hibler* [1997]. Fluxes of momentum into ice due to the overlying atmospheric winds and momentum fluxes between sea-ice and the ocean are calculated by solving for the momentum balance at each surface grid column [*Hibler and Bryan*, 1987].

2.2. Ocean Biogeochemical Model

[6] We overlay the Arctic Ocean circulation model with a biogeochemical model which carries six tracers: DIC, total alkalinity, phosphate (PO_4), dissolved organic phosphorus (DOP), dissolved oxygen, and RDOC. The biogeochemical model used in this study does not implement an ecosystem component as other biogeochemical models that are based on plankton functional types [*Le Quéré et al.*, 2005]. This approach has been adopted in order to significantly improve the computational speed given the high horizontal resolution of the physical modeling framework. The tracers are transported by the modeled circulation and mixing processes, and undergo biological and chemical transformations using parameterizations as applied in previous global modeling studies. More details of the biogeochemical model and parameterizations are provided in Appendix A. The prognostic equation for DIC, the key variable, is

$$\frac{\partial DIC}{\partial t} = -u\cdot\nabla DIC + \nabla\cdot K\nabla DIC + S_{DIC} + \frac{RDOC}{\tau}, \quad (1)$$

where the first two terms on the right represent advection and parameterized sub-gridscale mixing. Here S_{DIC} reflects the sources and sinks of carbon to and from a water parcel including biological consumption and remineralization of organic particles in the pelagic environment and non-riverine DOC (linked to the cycling of phosphorus by fixed elemental ratios) due to *in situ* marine processes as well as the air-sea exchange of CO_2 (see Appendix A). A complete description of this biogeochemical model is given by *Dutkiewicz et al.* [2002].

[7] We have assumed that DOC produced *in situ* is directly linked to the production and remineralization of DOP through a fixed elemental ratio (see Appendix A for further details). RDOC is treated independently (following *Manizza et al.* [2009]) and, without sufficient data to suggest otherwise, we neglect riverine contributions to DOP and PO_4. The e-folding timescale τ, provides a simplified parameterization of RDOC degradation. Distributions of DIC and alkalinity are initialized using empirical relationships based on physical quantities (see Appendix B for details), phosphate is initialized from the World Ocean Atlas [*Conkright et al.*, 2002] and oxygen and DOP are initialized using solutions from prior, equilibrated model integrations.

[8] The prognostic equation for RDOC

$$\frac{\partial RDOC}{\partial t} = -u\cdot\nabla RDOC + \nabla\cdot K\nabla RDOC + S_{RDOC} - \frac{RDOC}{\tau}, \quad (2)$$

includes representations of advection and mixing, a source term (S_{RDOC}) reflecting the time-varying riverine discharge [*Manizza et al.*, 2009] and the loss due to degradation processes ($-\frac{RDOC}{\tau}$: see above). The source term, S_{RDOC}, is imposed (following *Manizza et al.* [2009]) based on seasonally-explicit regression relationships which use co-variations between water yield and DOC concentrations in Arctic rivers to define RDOC input climatologies for 10 regions around the Pan-Arctic domain. These regions were defined to be the Barents Sea, Kara Sea, Laptev Sea, East Siberian Sea, Chukchi Sea, Bering Strait, Beaufort Sea, Canadian Archipelago, Hudson Bay and Hudson Strait using published watershed areas and seasonal water runoff [*Lammers et al.*, 2001]. Data from the Yukon, Mackenzie, and Kuparuk rivers were used to define a runoff-[DOC]

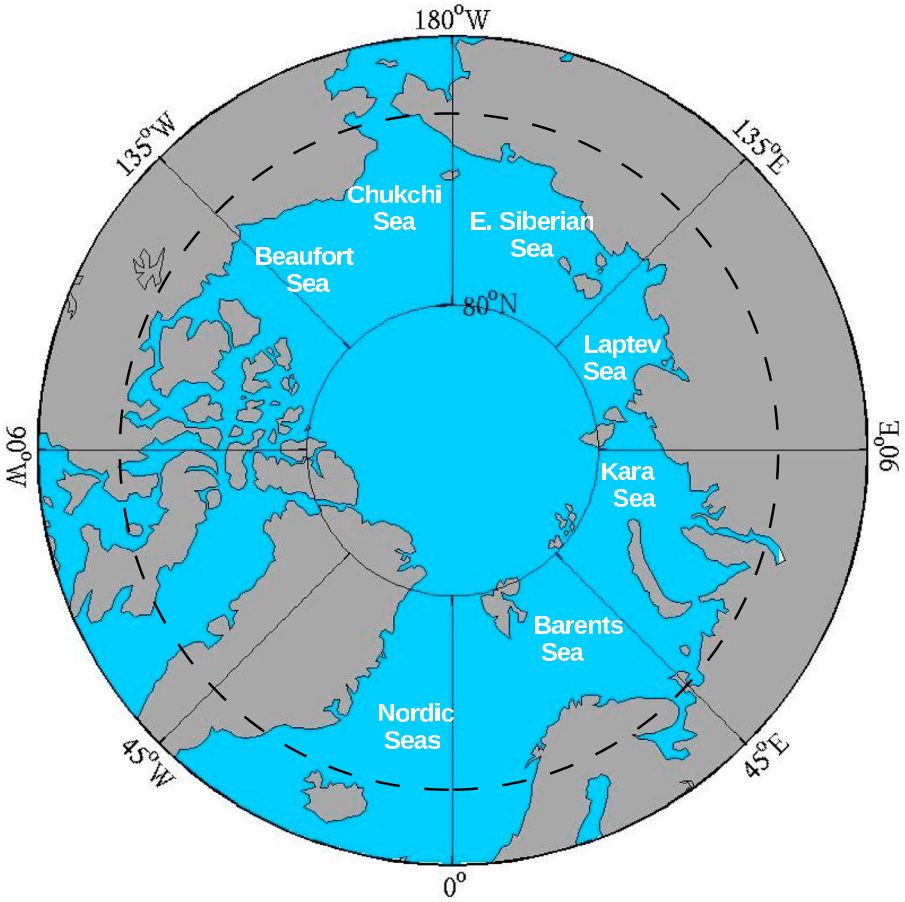

Figure 1. Map of the Arctic Ocean with most representative sectors. The black dashed line corresponds to the 65°N latitudinal boundary.

relationship for drainage areas in North America, and data from the Ob', Yenisey and Lena rivers were used to define a runoff-[DOC] relationship for drainage areas in Eurasia. Recent sampling efforts on these rivers have provided exceptional seasonal coverage [*McClelland et al.*, 2008] and the total, annual discharge of RDOC in the model is 37.7 Tg C a^{-1}, consistent with the estimate of *Raymond et al.* [2007]. Riverine particulate organic carbon (RPOC) is also an important carbon source to some regions of the Arctic Ocean. However, at the pan-arctic scale this flux is relatively small (~6 Tg C a^{-1}, [*McGuire et al.*, 2009]) compared to the flux of RDOC. Thus, with respect to terrestrial organic matter inputs, we have chosen to focus our attention on RDOC.

2.3. Suite of Model Integrations

[9] We examine a suite of four simulations in which the circulation and carbon cycle model are identical except for the source and degradation rate of RDOC. In the "control" simulation ("*riverine flux 10*", RF_{10}), we impose a realistic riverine source of terrigenous DOC with a degradation e-folding time-scale τ of 10 years with which the model reproduces observed DOC-salinity relationships [*Manizza et al.*, 2009]. We also perform a reference simulation ("*no river flux*", NRF), in which we set the riverine source of terrigenous DOC to zero and two additional sensitivity studies ("*riverine flux 5*", RF_5, and "*riverine flux 1*", RF_1) where τ is set to 5 and 1 years respectively. In all of the numerical experiments, we impose a uniform, non-seasonal atmospheric CO_2 mixing ratio of 354 ppm, representative of the 1990's, corresponding to the era of our physical simulation (1992–2001). We spin up the model for two decades, after which time the surface ocean and the thermocline of the modeled Arctic basin are close to steady state. We repeated the same 1992–2001 decade of forcing twice by using the final state of the physical and biogeochemical tracers obtained after the first decade to initialize the model for the second run. The length of our simulation allows us to obtain reliable results because on the shelf areas the residence time of the waters (<3 years, [*Macdonald et al.*, 1993]) is significantly less than our run.

3. Results: Arctic Ocean Carbon Cycle and Fluxes

[10] We discuss the region north of 65°N (Figure 1) in the simulations to avoid features strongly controlled by the boundary conditions, although the limit of the full domain is ~55°N. First, we discuss the large-scale surface distributions of biogeochemical tracers and the seasonal cycle of surface pCO_2 for key regions of the Arctic Ocean in the light of observed data. Second, we use the model to consider the sensitivity of the Arctic Ocean carbon cycle to the source of RDOC and its lability.

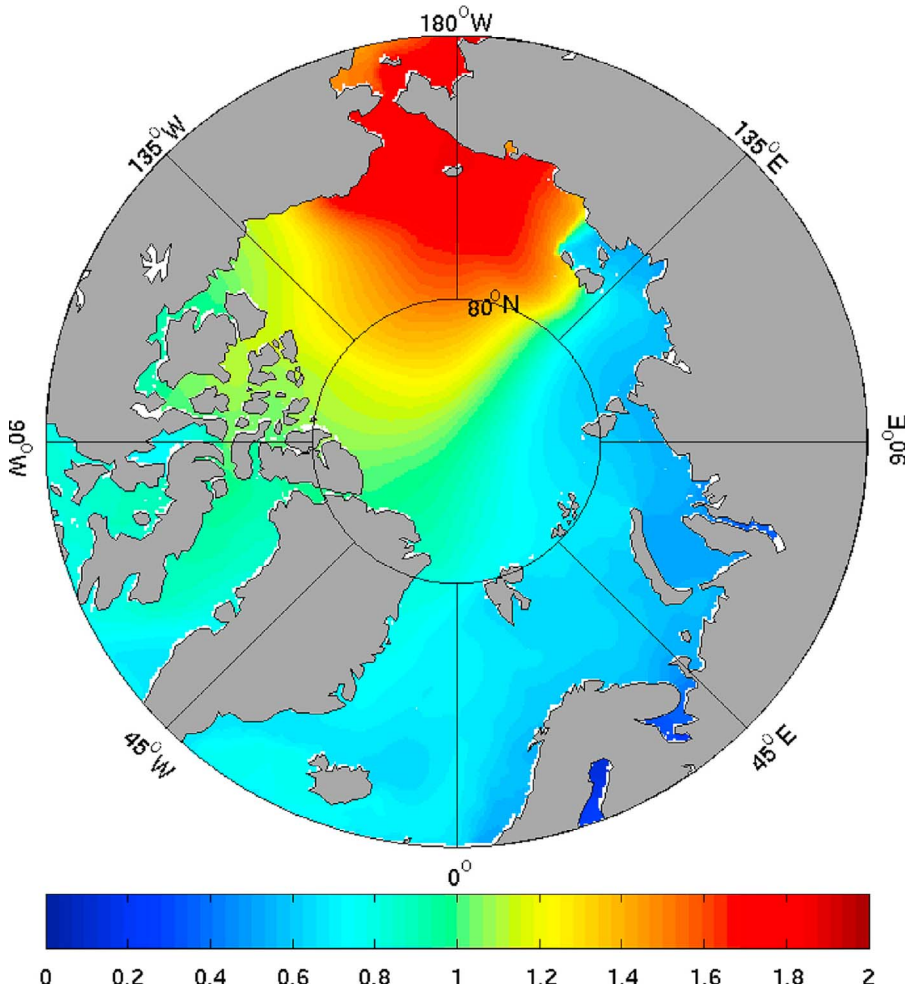

Figure 2. Annual average of surface [PO_4] obtained from the biogeochemical model in the the simulation RF_{10}. Units are μM.

3.1. Basin-Scale Distributions of Biogeochemical Tracers

[11] Here we compare the spatial distribution of modeled, surface ocean tracers with the available observations including the Carbon Dioxide in the Atlantic (CARINA) data set [*Jutterström et al.*, 2010]. We discuss the model solutions from the control simulation, RF_{10}, where the imposed remineralization e-folding time-scale τ (where τ corresponds to 10 years) produces realistic RDOC-salinity relationships [*Manizza et al.*, 2009].

[12] Many of the modeled tracer distributions have a strong imprint of the circulation and water mass structure in the surface Arctic Ocean, as is also evident in the compiled observations. For example, both modeled and observed surface distributions of [PO_4] (Figures 2 and 3) show a distinct signature of nutrient rich, Pacific waters entering the Arctic basin through the Bering Strait, where modeled [PO_4] reaches $\sim$1.8 μmol L^{-1}, higher than observed concentrations which are mostly summer values obtained when sea-ice melts and biological production is active. The phosphate rich surface waters of Pacific origin spread towards both the central and the western parts of the basin through the Canadian Archipelago [*McLaughlin et al.*, 1996; *Steele et al.*, 2004]. In contrast, both model and observations indicate that [PO_4] is relatively low in the eastern Arctic Ocean ($\leq$0.8 μmol L^{-1}; Figures 2 and 3), reflecting the inflow of nutrient depleted waters originating in the North Atlantic. This is consistent with observations from the Nordic Seas [e.g., *Falck and Anderson*, 2005].

[13] The surface distribution of Alkalinity (ALK) in our model (Figure 4, right) reflects the surface distribution of sea surface salinity (illustrated by *Manizza et al.* [2009]) exhibiting saline, surface North Atlantic waters, with ALK exceeding 2200 μmol kg^{-1}, entering the Arctic Ocean basin through the Nordic Seas as is observed though with even higher concentrations than in the model (Figure 5, right). Regions of the model Arctic strongly influenced by

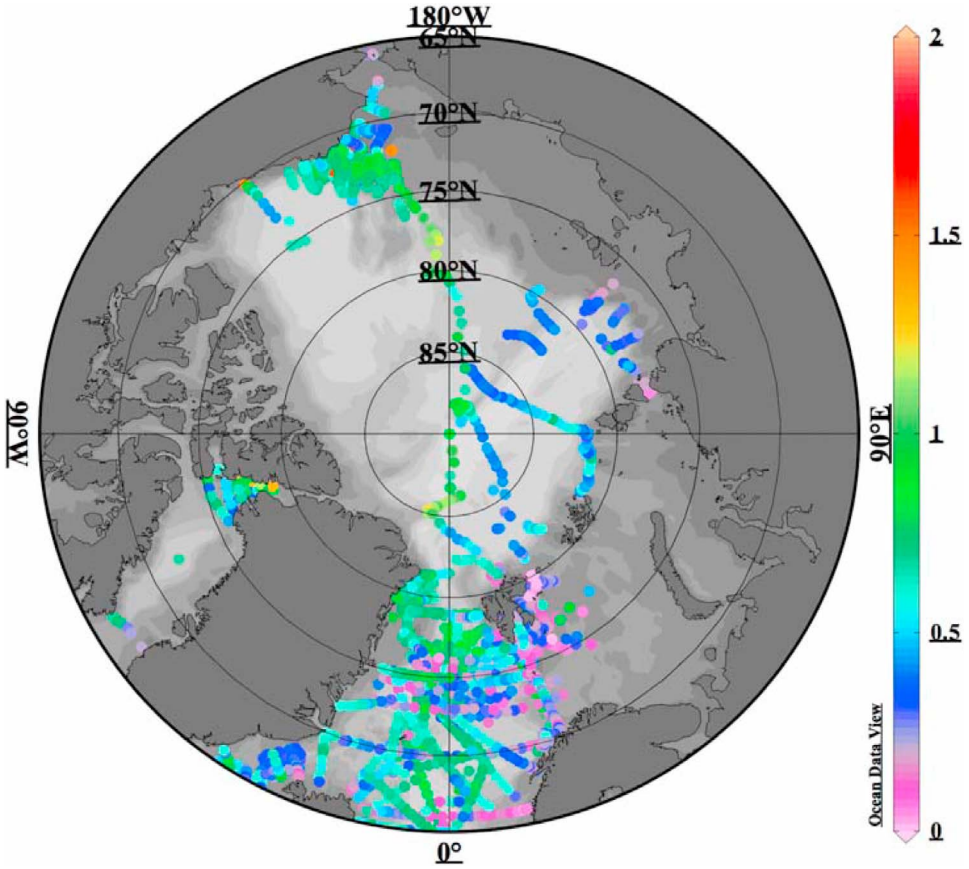

Figure 3. Surface [PO_4] from oceanic observations obtained from the CARINA data set. Units are μM.

freshwater runoff, such as the Eurasian continental shelf, Chukchi Sea, and the narrow shelf in the Western Arctic near the mouth of the Mackenzie River (Figure 4, right) show correspondingly dilute values of surface ALK (less than 2000 μmol kg^{-1}). These low values are comparable to those observed in the Western Arctic by *Bates* [2006] and in the Siberian Shelf Seas as reported by *Olsson and Anderson* [1997]. The model's large-scale distribution of surface ALK is qualitatively consistent with the observed gradients revealed in the CARINA data compilation (Figure 5, right).

[14] In the control simulation (RF_{10}) there are high surface concentrations of RDOC (greater than 100 μM) along the shelf, close to the river mouths, and a strong decrease towards the interior of the basin (Figure 6, left) due to dilution with waters imported from the Pacific and Atlantic as well as microbial degradation.

[15] The simulated surface distribution of DIC (Figure 4, left) also reflects the large scale surface circulation, with higher concentrations (~2030 μmol kg^{-1}) associated with a tongue of cool, salty and high alkalinity North Atlantic water entering the Arctic basin along the Norwegian coast and continuing through the Barents Sea (Figure 4, left). Lower values of DIC (~1850 μmol kg^{-1}) reflect the passage of Pacific waters which enter through the Bering Strait. These broad-scale features of the simulation (Figure 4, left) are qualitatively consistent with the CARINA compilation of observations (Figure 5, left). The modeled concentrations in the Nordic Seas are also corroborated by data collected in the same area by *Falck and Anderson* [2005]. Along both the Eurasian and the North American coastal zones, surface [DIC] is relatively low (~1850 μmol kg^{-1}) due to dilution by the significant riverine freshwater input. In the center of the basin surface DIC is elevated (up to ~2080 μmol kg^{-1}) due to the remineralization of RDOC and persistent sea-ice cover, which inhibits outgassing of CO_2 to the atmosphere (Figure 4, left). In the regions of seasonal sea-ice cover, including the Chukchi and the Beaufort Seas, intense biological productivity in the model draws surface DIC down to

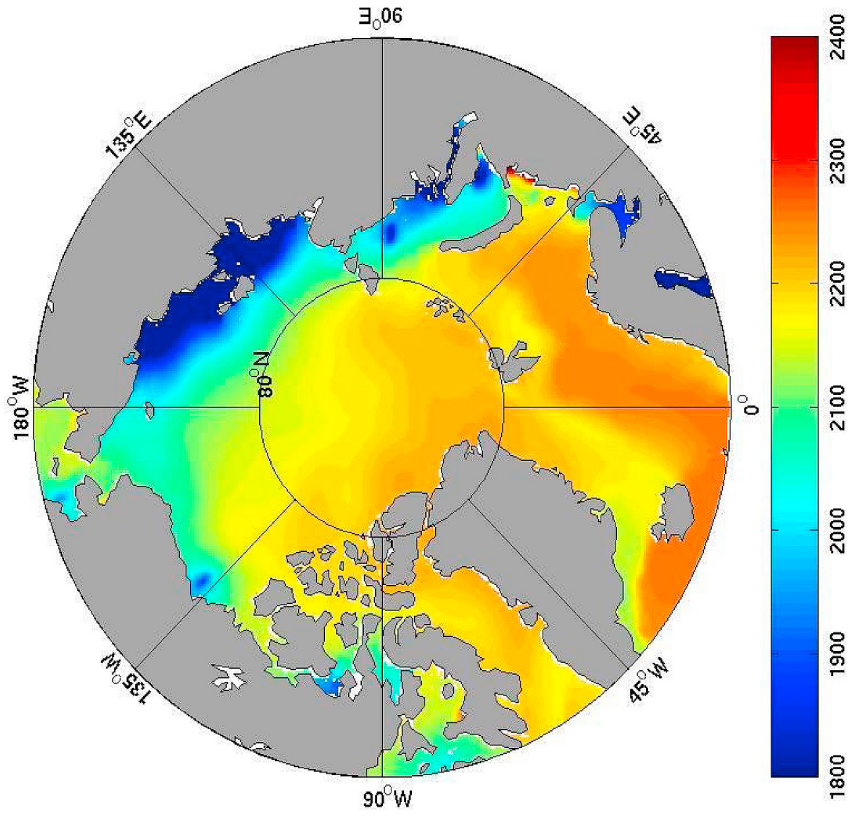

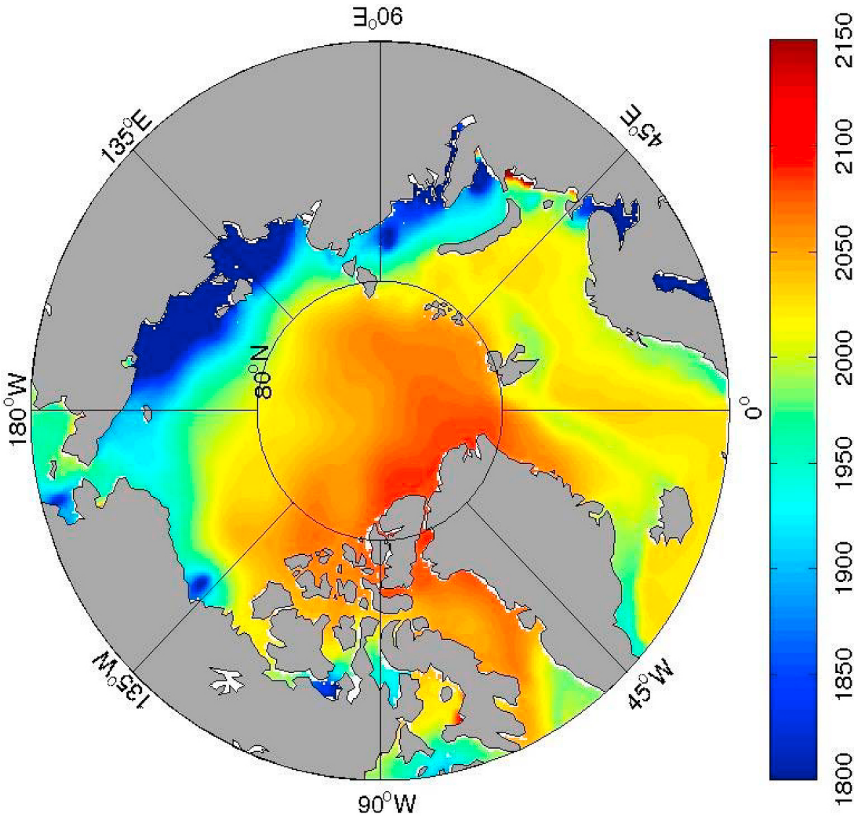

Figure 4. Surface distribution of (left) DIC and (right) alkalinity computed by the biogeochemical model in the simulation RF_{10}. Units are μmol kg^{-1}.

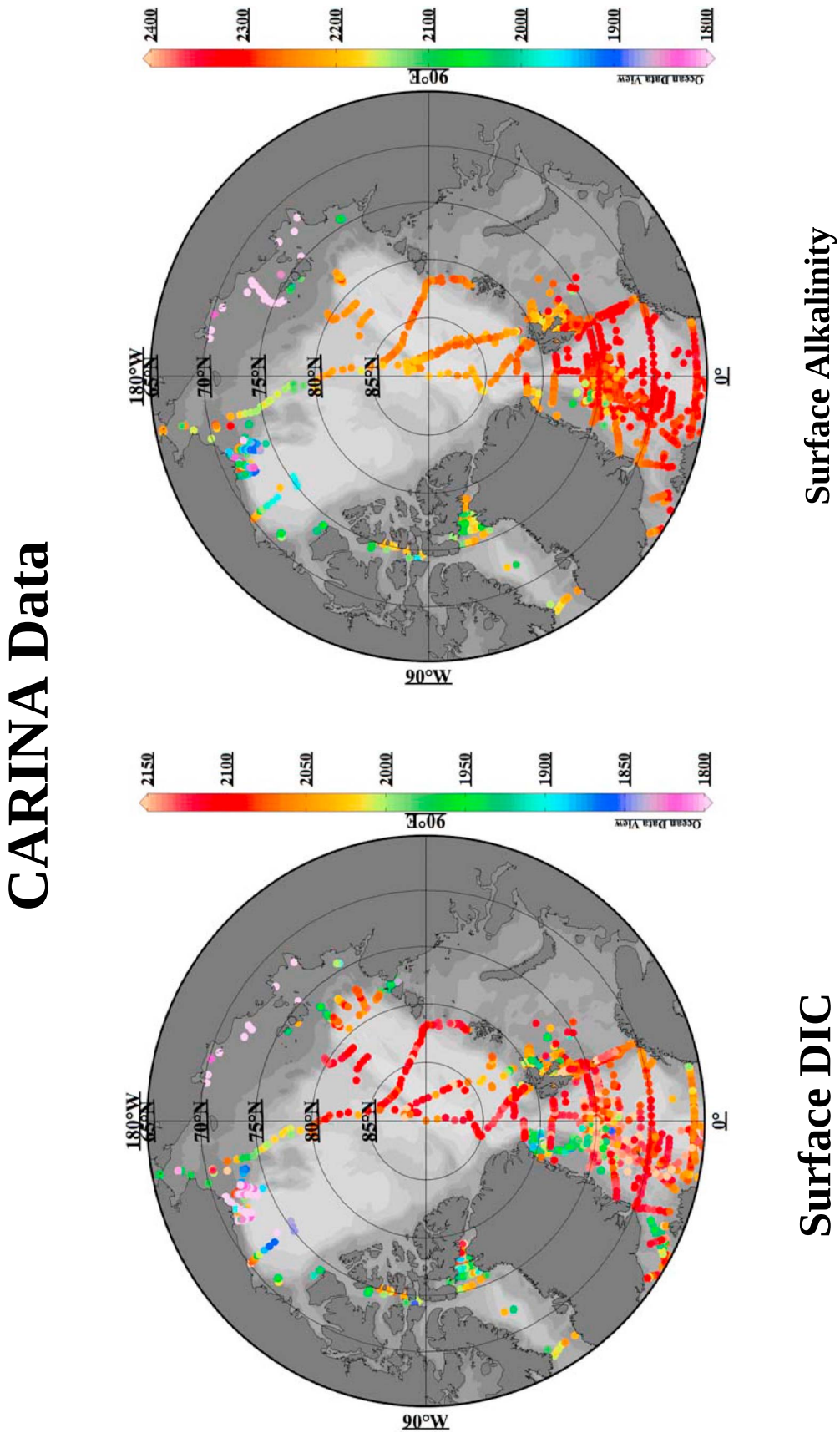

Figure 5. Annual average of (left) surface DIC and (right) surface alkalinity from available observations from the CARINA data set. Units are μmol kg^{-1}.

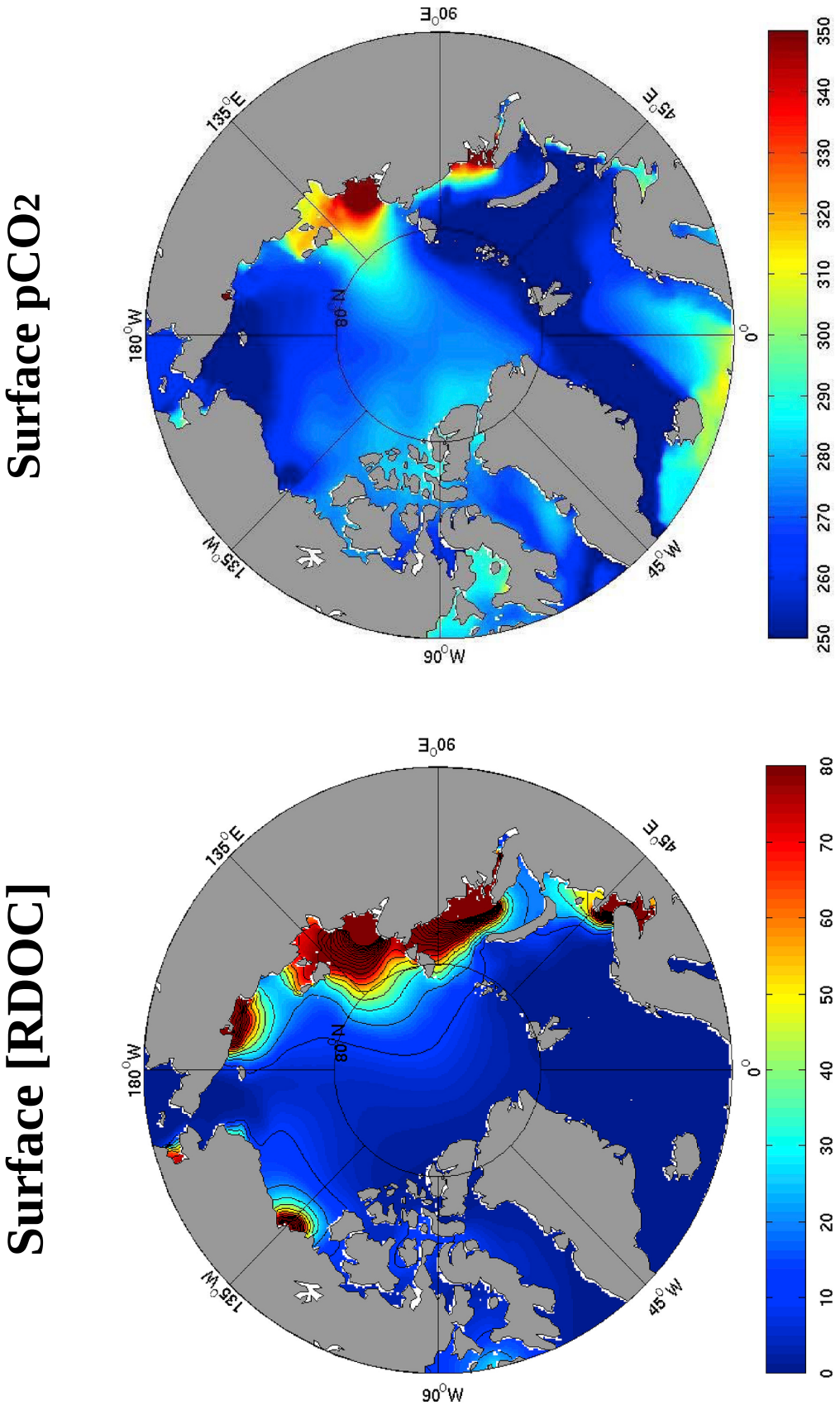

Figure 6. Annual average of (left) surface [RDOC] and (right) surface ocean pCO_2 computed by the biogeochemical model in the simulation RF_{10}. Note that color scale saturates for values greater than 350 μatm. Units are μM (Figure 6, left) and μatm (Figure 6, right).

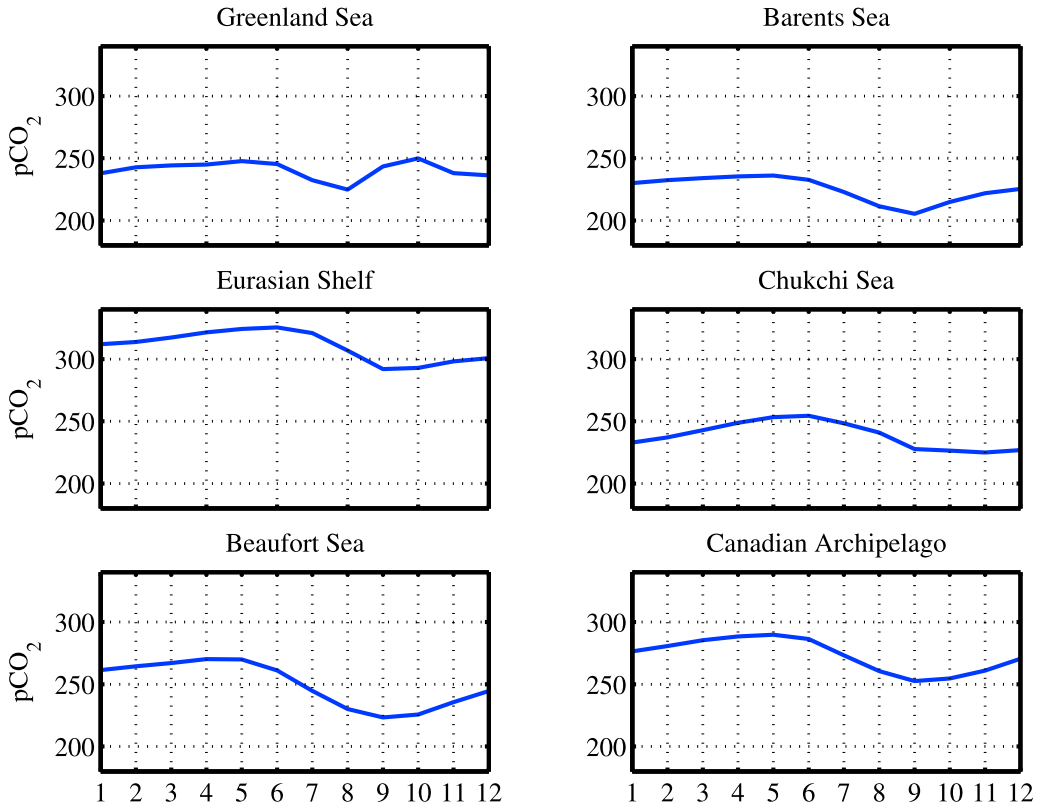

Figure 7. Seasonal cycle of surface ocean pCO_2 in six locations of the Arctic Ocean from the RF_{10} simulation. For each location, each monthly value is averaged over a selected area of 10 by 10 grid points. Units are μatm.

1850–1900 μmol kg^{-1}, comparable to observed values from the same area [*Bates*, 2006] and the CARINA compilation (Figure 5, left).

3.2. Surface Ocean pCO_2

[16] In the Arctic Ocean three main factors contribute to maintain values of surface pCO_2 relatively low (and undersaturated with respect to atmospheric [CO_2]) in most of the areas: (1) the low temperature of seawater, (2) the extensive sea-ice cover that caps the central area of the Arctic basin limiting the air-sea gas exchange of CO_2, and (3) the biological carbon uptake by phytoplankton regulated by the seasonal melting of sea-ice cover occurring mostly over the shelf areas. Nevertheless, the relatively sparse published measurements indicate higher values of surface ocean pCO_2 in the Eurasian sector and lower values in the North-American sector. This gradient is qualitatively captured in the model solutions (Figure 6, right).

[17] The mechanisms underlying modeled seasonal variations of pCO_2 will be discussed with special focus on six regions of the Arctic (Figure 7): (1) the Greenland Sea, (2) the Barents Sea, (3) the Eurasian Shelf, (4) the Chukchi Sea, (5) the Beaufort Sea, (6) the Canadian Archipelago.

[18] In the Greenland Sea, modeled surface pCO_2 varies strongly with season, with a spring and summer minimum of less than 250 μatm (Figure 7). The seasonal cycle is strongly affected by sea ice: during the winter, ice traps respired CO_2 in the surface waters. In spring and summer, the retreat of the ice and warming stimulate primary production drawing down surface DIC and pCO_2 despite the reduction in solubility.

[19] In the modeled Barents Sea, surface pCO_2 is drawn down during the late summer, from 225 μatm by $\sim$25 μatm, again reflecting the control of DIC by primary production, insolation and sea-ice, which over-ride the seasonal variations in solubility. This is consistent with the observed seasonal cycle of surface ocean pCO_2 from several field studies [*Nakaoka et al.*, 2006; *Omar et al.*, 2007] although our model underestimates their observed values by $\sim$50 μatm. This could be due to an excessive biological drawdown of DIC in our model although this model-data mismatch has not been investigated in great detail.

[20] On the Eurasian Shelf, the modeled seasonality of surface ocean pCO_2 is dominated by the influence of sea-ice and remineralization of RDOC. The source of RDOC has a sharp peak in the spring-summer due to river run-off [*Manizza et al.*, 2009] and makes the surface ocean pCO_2 reach values of $\sim$300 μatm on the Eurasian shelf in our model. In the areas of the Eurasian shelf in the very proximity of the coast, where the input of RDOC occurs (Figure 6, left) the values of surface ocean pCO_2 exceed 350 μatm (Figure 6, right) causing CO_2 outgassing in those areas (Figure 8). The extremely high values of surface ocean pCO_2 exceeding the atmospheric values are also consistent with the findings of *Anderson et al.* [2009].

[21] In the Chukchi Sea, the model is typically undersaturated (less than 250 μatm) due to the efficient biological

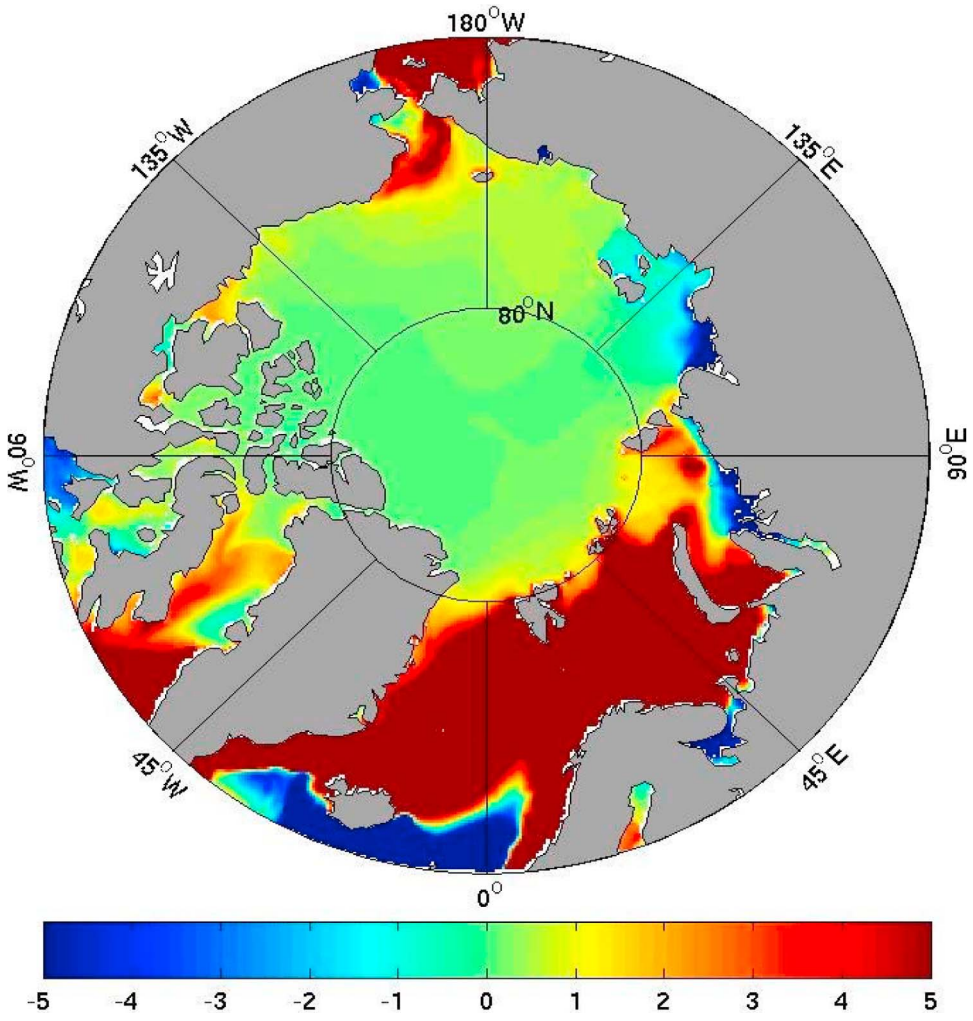

Figure 8. Annual average of air-sea CO_2 fluxes for the RF_{10} simulation. Units are g C m^{-2} a^{-1} and negative values indicate outgassing.

pump in the ice-free months (Figure 7), fueled by the nutrient-rich waters from the North Pacific Ocean (Figure 2). Again, the model's seasonal values are in fair agreement with existing data [*Semiletov*, 1999; *Pipko et al.*, 2002; *Murata and Takizawa*, 2003; *Bates*, 2006; *Fransson et al.*, 2002] ranging between 150 and 300 μatm although our model never reaches the drastic summer minimum value of pCO_2 of 150 μatm as observed in those studies during the ice-free months.

[22] On the Beaufort Sea shelf, reported surface ocean pCO_2 is usually lower than 300 μatm [*Murata and Takizawa*, 2003; *Bates*, 2006; *Mucci et al.*, 2010] with higher values observed in the Canadian Archipelago [*Miller et al.*, 2002]. Consistently, pCO_2 is generally lower in the model's Beaufort Sea than Canadian Archipelago, although the contrast is less than that observed. The model suggests a similar seasonal cycle of surface ocean pCO_2 in the two areas, dominated by biological drawdown and under-saturation during the ice-free period. In the Canadian Archipelago the biogeochemical model underestimates the spring values of surface ocean pCO_2 (~300 μatm) when compared to observations (400–450 μatm [*Miller et al.*, 2002]) but captures the summer values (200-250 μatm) due to the biologically-driven drawdown reported in the same study.

[23] Overall, the biogeochemical model captures the broad gradients of surface ocean pCO_2 as suggested by observations. It is important to note that it captures the clear difference in surface ocean pCO_2 between the Eurasian and North-American basins only when we explicitly represent the effect of remineralized RDOC on the oceanic pool of DIC and consequently on oceanic pCO_2, confirming the crucial role of land-ocean coupling in the functioning of the Arctic Ocean carbon cycle.

3.3. Arctic Ocean Circulation, Riverine DOC Delivery and Air-Sea CO_2 Fluxes

[24] The available data and model solutions suggest a strong role for circulation and transport, as well as riverine

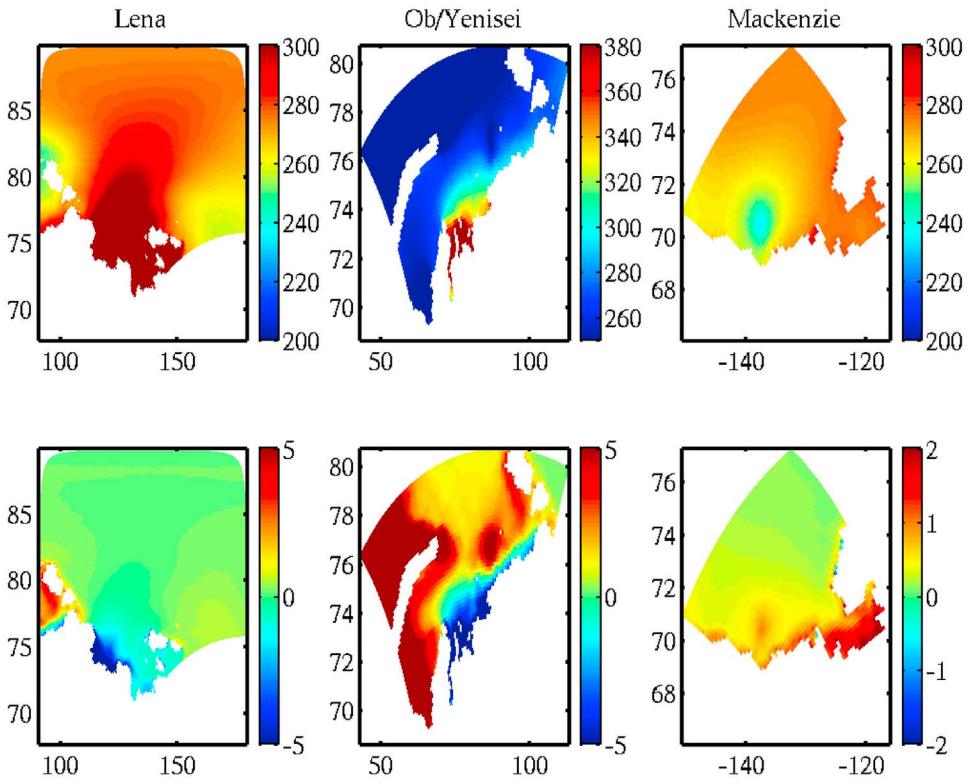

Figure 9. Annual average of (top) surface pCO_2 and (bottom) air-sea CO_2 fluxes computed by the biogeochemical model in the simulation RF_{10} on three coastal locations of the Arctic Ocean where major RDOC discharge occurs. Units are μatm (Figure 9, top), g C m^{-2} a^{-1} (Figure 9, bottom), and positive values of air-sea CO_2 fluxes indicate ingassing. Note that different scales are used for Eurasian and North-American Arctic Ocean coastal zones.

delivery of organic carbon, in regulating the regional patterns of air-sea flux in the Arctic.

[25] In the eastern region of the Nordic Seas (the Norwegian Sea) that is almost permanently ice-free surface DIC-rich waters, originating in the North Atlantic and traveling northward, progressively cool and take up CO_2 due to the effect of the solubility pump. Cooling and relatively ice-free circumstances drive a significant ocean CO_2 uptake of about 20 g C m^{-2} a^{-1} in the Nordic Seas (Figure 8). This is consistent in sign with what inferred by *Skjelvan et al.* [2005] (40 g C m^{-2} a^{-1}) based on observations although our model would suggest a weaker CO_2 sink.

[26] In the coastal zones of the Eurasian Shelves, surface ocean pCO_2 (Figure 6, right) exceeds the imposed atmospheric pCO_2 of 354 ppm, associated with the remineralization of RDOC which enhances DIC. The source of DIC from RDOC is strong enough in this region to drive an outgassing of CO_2 in the model ($\sim$10 g C m^{-2} a^{-1}) in contrast to the uptake which characterizes most of the basin. These model results are also in agreement with the recent findings shown by *Anderson et al.* [2009] for the Siberian Shelf Seas. The area including the Eastern Siberian Sea, Chukchi Sea, and the coastal Beaufort Sea represent a region of CO_2 uptake for the Arctic Ocean. In these zones, the values of surface ocean pCO_2 are maintained low due to the *in-situ* biological drawdown of DIC as shown in the previous section where pCO_2 was discussed. In fact the seasonal melting of sea-ice allows the co-utilization of nutrients and solar radiation to fuel photosynthetic activity so that these oceanic areas vigorously take up CO_2 from the atmosphere (>10 g C m^{-2} a^{-1}).

[27] In the case of the Beaufort Sea, our biogeochemical model shows this area is a net sink of CO_2 (Figure 8). Low concentrations of RDOC in the Beaufort Gyre (both modeled and observed) reflect a combination of dilution and microbial degradation effects. Closer to shore, Mackenzie River RDOC has a significant influence on surface pCO_2 (Figure 6, right), but this contribution of RDOC is not enough to drive a clear outgassing effect (Figure 8). We have shown above that freshwater discharge causes a dilution of DIC and ALK (Figures 4 and 5). This dilution effect, which lowers the values of surface ocean pCO_2, is stronger than the RDOC respiration effect associated with the Mackenzie River input. This contrasts sharply with model results on the Eurasian side (Figure 9), where degradation of RDOC clearly dominates over the dilution effect. However, the Mackenzie River is unique among the major arctic rivers in having a RPOC flux that is comparable to its RDOC flux [*McGuire et al.*, 2009]. Thus, by not including RPOC in the model it is likely that we are substantially underestimating the influence of Mackenzie River inputs on the carbon balance of coastal waters in the Beaufort Sea region.

[28] Another aspect that is not taken into account in our biogechemical model is the potential influence of the input of terrestrial carbon due to coastal erosion, particularly significant in the Beaufort Sea [*Ping et al.*, 2011]. Along the Beaufort Sea coast the flux of total organic carbon from

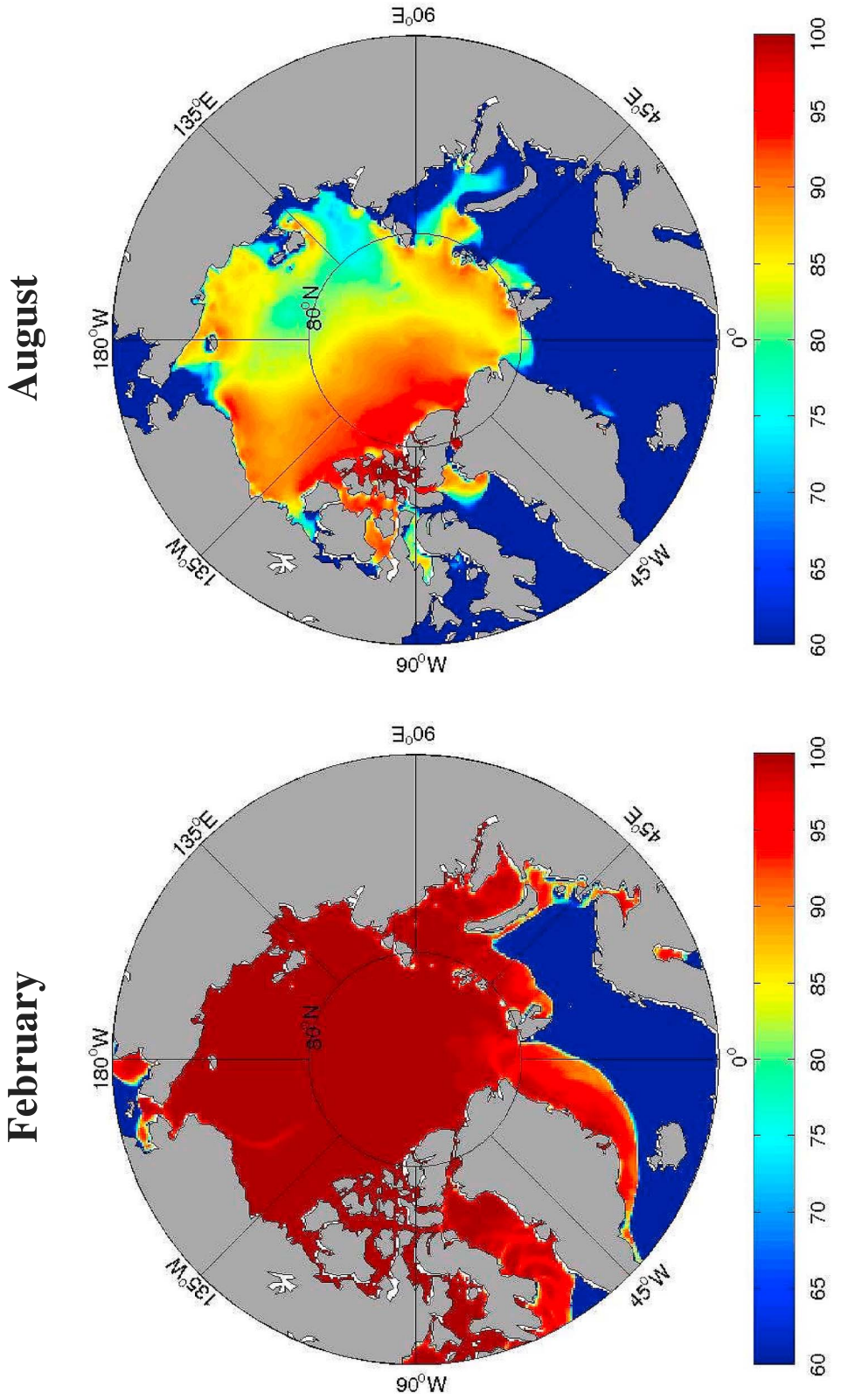

Figure 10. Distribution of sea-ice cover in (left) February and (right) August. Units are %.

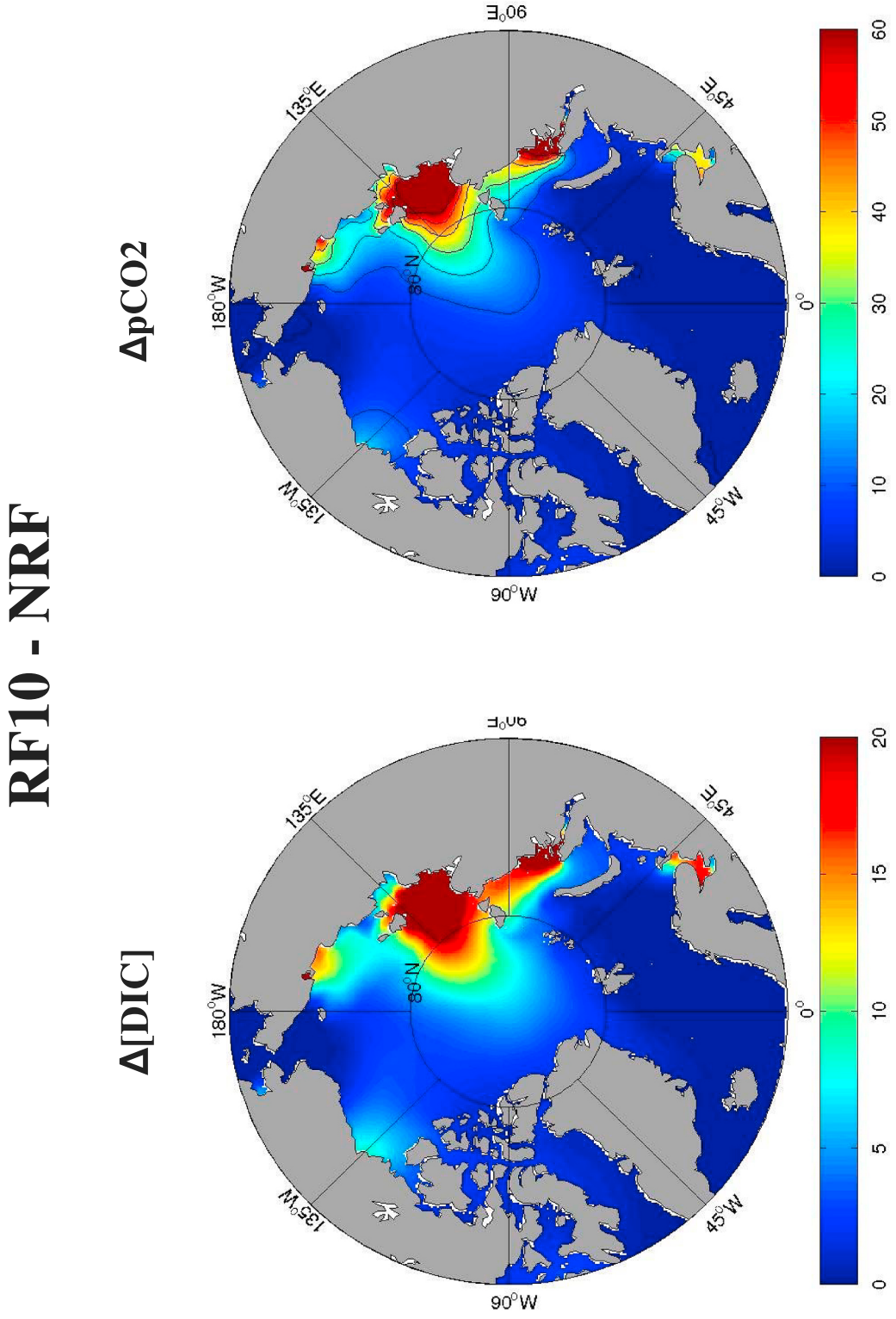

Figure 11. Annual average of difference in (left) surface DIC and (right) pCO_2 between RF_{10} and NRF. Units are μmol kg^{-1} (Figure 11, left) and μatm (Figure 11, right).

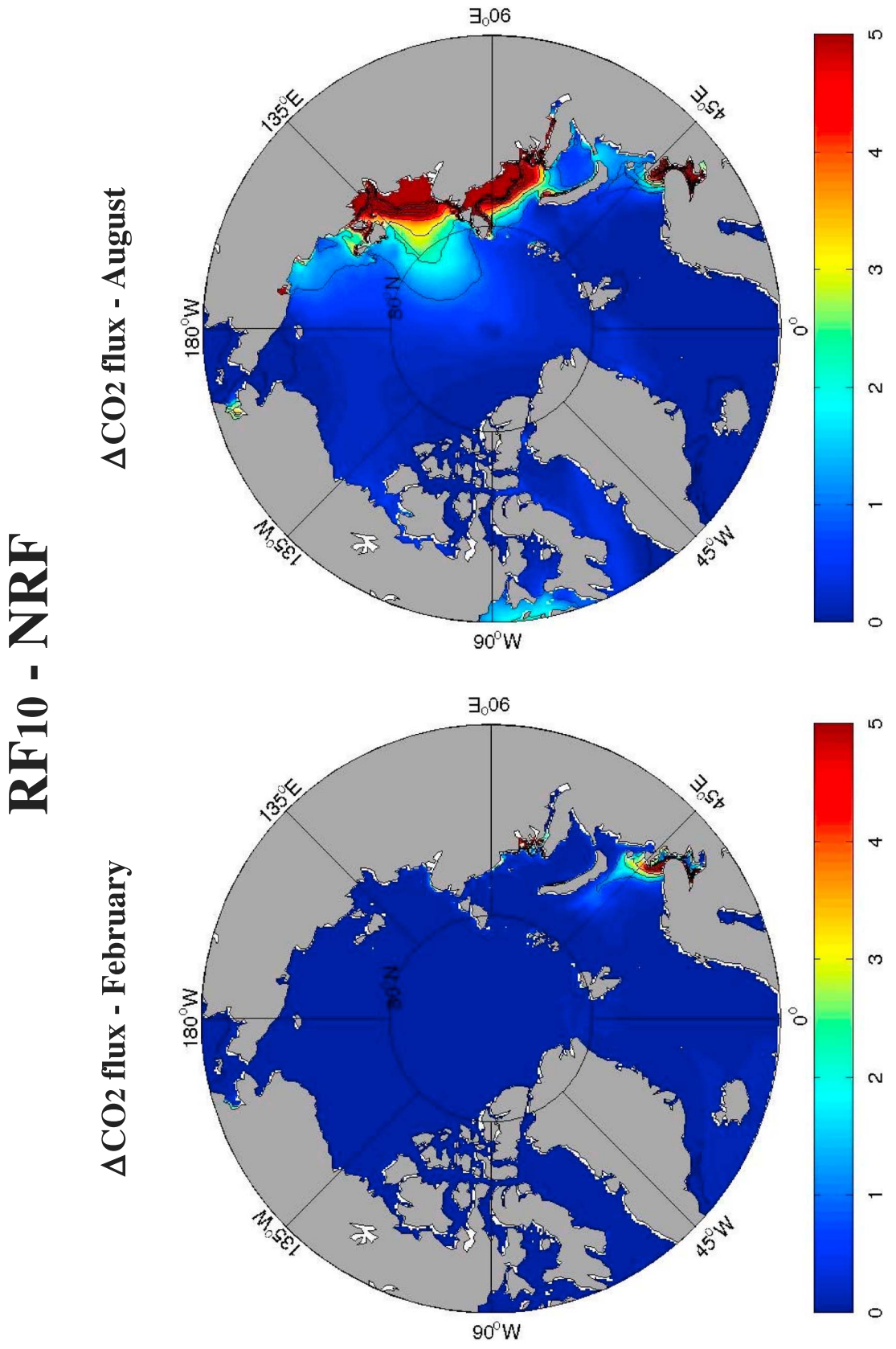

Figure 12. Difference in air-sea CO_2 fluxes in (left) February and (right) August between RF_{10} and NRF. Units are g C m^{-2} a^{-1} and positive values correspond to outgassing.

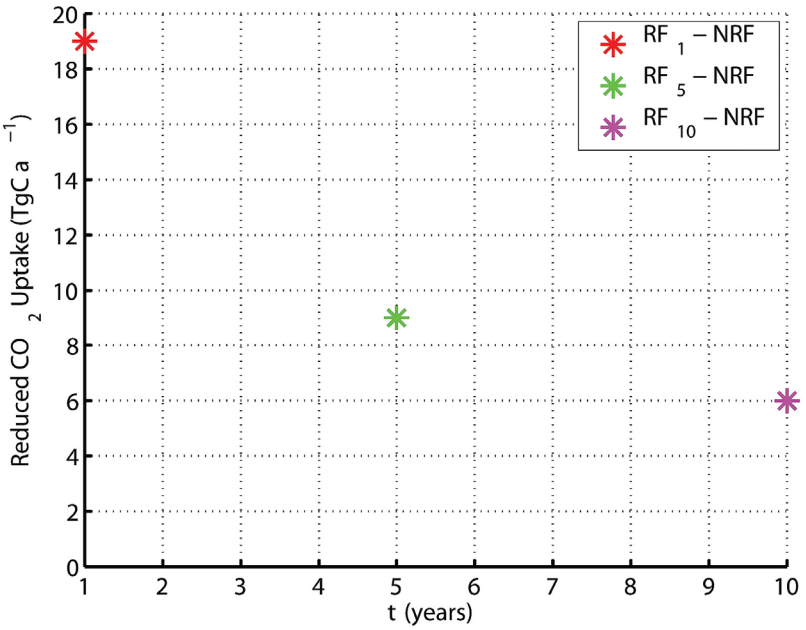

Figure 13. Relationship between τ and change in CO_2 uptake of RF_{10}, RF_5, and RF_1 compared to NRF. Individual values of oceanic CO_2 uptake used to calculate differences shown here are reported in Table 1.

coastal erosion is estimated to be ~0.09 Tg C a^{-1} [*Stein and MacDonald*, 2003]. This input in relatively small compared to a total organic carbon input of ~4.1 Tg C a^{-1} from the Mackenzie River [*Stein and MacDonald*, 2003]. The lack of the RPOC flux could in theory impact the results shown in this study for the Beaufort Sea. However, the Beaufort Sea is estimated to be an area corresponding to a CO_2 sink for the Arctic Ocean [*Bates and Mathis*, 2009], as also confirmed by our results, and the remarkable difference with carbon cycle response of the Eurasian shelf can be simply explained by the different magnitude of the RDOC flux on the two shelf sea areas [*Manizza et al.*, 2009].

[29] In the region corresponding to Baffin Bay and its northernmost area (the North Water) the biogeochemical model predominantly shows a CO_2 sink (Figure 8). The southernmost region of Baffin Bay shows a clear uptake of CO_2 (3 g C m^{-2} a^{-1}) that is mostly determined by the seasonal and substantial reduction of sea-ice cover (Figure 10) that allows the co-utilization of light and nutrients and the biological drawdown of DIC. However, in the North Water the magnitude of the CO_2 uptake is less than that computed for the rest of Baffin Bay. In this particular area of the Arctic Ocean adjacent to the Canadian Archipelago a seasonal summer polynya, extensively observed and documented by field studies, allows the utilization of macronutrients and the subsequent biological drawdown of DIC. It could be possible that our model does not correctly reproduce this drastic seasonal reduction of the sea-ice cover in that area between Greenland and the Canadian Archipelago, also shown in this study (Figure 10), so that the annual mean value of CO_2 uptake is ~1 g C m^{-2} a^{-1}, less then in the rest of Baffin Bay.

[30] Although we did not consider Hudson Bay in our carbon budget of the Arctic Ocean because it is out of our geographical limit (65°N), in our biogeochemical model we did have an explicit representation of the source of RDOC discharging into this semi-enclosed oceanic region, as also shown in our previous study [*Manizza et al.*, 2009]. The discharge of RDOC makes this area a net carbon source for the atmosphere. In fact, our biogeochemical model calculates a net CO_2 outgassing up to 1 g C m^{-2} a^{-1} as annual average.

[31] The effect of RDOC inputs on the regional ocean carbon system is illustrated by the difference in surface DIC between the integrations with and without riverine source (RF_{10} and NRF; Figure 11). As expected, the largest impact (~20 μmol kg^{-1}) is in the coastal areas near the sources of RDOC, elevating pCO_2 by as much as 60 μatm relative to the case without an RDOC source (Figure 11, right) and effectively reversing the direction of the air-sea flux. In the center of the basin, the DIC generated by RDOC respiration is trapped and accumulates under the more persistent sea-ice (Figure 10). However, the accumulated DIC derived from RDOC (5–10 μmol kg^{-1}) is less than in the coastal areas because of dilution with open ocean waters imported to the region by the Transpolar Drift via mixing and advective processes.

[32] The response of the air-sea CO_2 flux to the RDOC source is strongly regulated by the seasonal cycle of sea-ice cover. In winter, sea-ice inhibits fluxes in both model integrations (RF_{10} and NRF). In summer the reduction of sea-ice cover (Figure 10), particularly over the Eurasian and North American shelves, allows the outgassing of the excess CO_2 with a seasonal outgassing of up to 2 g C m^{-2} a^{-1} (Figure 12).

3.4. Sensitivity of the Arctic Ocean Carbon Cycle to RDOC Lability

[33] Integrated annually and over the area north of 65°N, the modeled Arctic Ocean takes up 59 Tg C a^{-1} across the sea surface in the model run where τ is equal to 10 years (RF_{10}). This is within the broad range of estimates based on extrapolation of observations by *Bates* [2006] (20–100 Tg C a^{-1}), and slightly below the more recent estimate by *Bates*

Table 1. Summary of the Simulations Carried Out for This Study[a]

Simulation	DIC/RDOC Coupling	τ (years)	CO_2 Uptake (Tg C a^{-1})	Reduced Uptake (%)
NRF	No	None	65	–
RF_{10}	Yes	10	59	9.2
RF_5	Yes	5	56	14
RF_1	Yes	1	46	30

[a]The "reduced uptake" as a percentage indicates the difference between each simulation that implements the DIC/RDOC coupling and the NRF simulation that is then divided by the CO_2 uptake of NRF.

and Mathis [2009] (66–199 Tg C a^{-1}). Differences in integrated annual, basin-wide uptake of CO_2 among the suite of numerical experiments with imposed RDOC source (RF_{10} - the "best" case, e-folding lifetime of 10 years for RDOC in the marine environment; RF_5 - RDOC e-folding lifetime of 5 years, and RF_1 - RDOC e-folding lifetime of 1 year) reveal an inverse relationship between RDOC e-folding lifetime τ and the net basin uptake of CO_2 (Figure 13). Basin wide net CO_2 uptake is 65, 59, 56, 46 Tg C a^{-1} for numerical experiments NRF (no RDOC flux), RF_{10}, RF_5, RF_1, respectively (Table 1). A shorter lifetime of RDOC leads to higher local surface DIC and pCO_2 reducing the net CO_2 uptake in the basin. With RDOC e-folding lifetime of about τ = 10 years (the most realistic scenario [*Hansell et al.*, 2004; *Manizza et al.*, 2009]) the CO_2 uptake of the Arctic Ocean is reduced by ~6 Tg C a^{-1}, almost 10% of the total, a significant contribution but not a first order control on the Arctic basin air-sea flux. If *all* of the RDOC were released to the atmosphere locally it would be an order one contribution, almost canceling the uptake due to cooling and biological drawdown. Thus, about 15% of the 38 Tg C of RDOC delivered annually to the Arctic basin is released to the atmosphere locally. The remaining 85% is transported as DOC, or subsurface DIC, into the Atlantic basin as also suggested by previous studies mostly by the advective processes mediated by the Eastern Greenland Current [*Benner et al.*, 2005] and by waters flowing out of the Arctic Ocean through the Canadian Archipelago. Some fraction of that will find its way into the deep water formation regions of the Nordic and Labrador Seas to be sequestered for centuries in the deep oceans.

4. Summary and Discussion

[34] We have employed a numerical model to simulate the marine carbon cycle in the present-day Arctic Ocean and to evaluate the role of RDOC flux in modulating the regional air-sea CO_2 flux. Our model would suggest that for present-day climatic conditions (when a climatic forcing corresponding to 1992–2002 is applied although we repeated the same forcing period twice to reach a steady state solution of our model) the Arctic Ocean CO_2 sink is 59 Tg C a^{-1} when a realistic RDOC flux and its data-constrained lability are fully taken into account. The model suggests that, though the total riverine delivery of carbon to the basin is of similar magnitude to the integrated carbon uptake, much of that terrigenous carbon is transported out of the Arctic, either as RDOC or DIC. However, about 15% does escape across the sea surface as CO_2 within the region, reducing the basin-scale carbon uptake by about 10%; a minor, though not negligible effect.

[35] The crude parameterization of transformation of RDOC into DIC used in this study and developed in our previous study [*Manizza et al.*, 2009] allowed us to realistically reproduce the observations although in a simplified way. The rate of conversion (τ^{-1}) of RDOC into DIC would represent altogether the effect of all the natural processes that in the Arctic Ocean contributes to this biogeochemical transformation, such as the remineralization carried out by heterotrophic bacteria and the photodegradation operated by sunlight mostly occurring during the summer months in the ice-free zones of the Arctic Ocean.

[36] In this study we only considered the flux of the RDOC while neglecting the flux of the RPOC. We think that the lack of this factor in the land-ocean coupling of the Arctic carbon cycle would not greatly impact our results, given that at basin scale the flux of RDOC is significantly larger than that of RPOC. However, we do recognize that RPOC may be a major regional consideration in some sectors of the Arctic Ocean such as the Beaufort Sea shelf near the Mackenzie River. Furthermore, our model did not have any sedimentary compartment that could represent the processes of sedimentation and, more important, re-suspension where this latter could enrich the water column in carbon and potentially affect then the air-sea gas exchange. Nevertheless, we think that this additional factor should not be crucial for the correct representation of the spatial gradient of surface ocean pCO_2 in the Arctic Ocean because even without a sedimentary model our biogeochemical model was able to capture the main spatial patterns derived from observations.

[37] Climate models projections predict that by the end of this century there could be an increase in surface air-temperature of up to 6°C [*Kattsov and Kallen*, 2005] in the polar regions. This will affect the Arctic Ocean temperatures, that already are showing clear signs of warming [*Steele et al.*, 2008], and the rates of metabolic processes in both ocean and terrestrial environments, possibly reducing the lifetime or RDOC in the ocean. The models also predict changes in the discharge of Arctic rivers [*Manabe et al.*, 2004] and signs of this change have already been detected [*Peterson et al.*, 2002]. Changes in discharge, along with permafrost dynamics, and terrestrial microbial response will no doubt modify the delivery of terrigenous DOC to the oceans [*Frey and McClelland*, 2009]. Models such as this provide a platform for both process-based and quantitative syntheses, as well as sensitivity studies, of productivity and the carbon cycle in the marine environment and its intimate links with the terrestrial carbon cycle in the Arctic. To consider sensitivity to climate change, we would need not only simulations of the physical environment but also more detailed and mechanistic models of the biological processes including not only primary producers but also the microbial respiration of terrigenous and marine organic matter. How would primary production change in response to a regional 6°C warming? Some clear signs of change in primary production to ocean warming and sea-ice reduction have been already detected [*Pabi et al.*, 2008; *Arrigo et al.*, 2008]. They would suggest that as sea-ice melting continues, the Arctic waters will increase their productivity with potential consequences for an enhancement in its CO_2 uptake [*Walsh*, 1989; *Bates et al.*, 2006; *McGuire et al.*, 2010]. Furthermore, how would microbial respiration rates change? Is their sensitivity decoupled? Reliable, prognostic models of these complex and (in some cases) poorly

understood processes are a desirable goal for climate change science but represent a significant challenge which will require significant and cooperative efforts to achieve.

[38] A continuous trend of reduction in sea-ice cover in the near future and the consequent expansion of ice-free ocean areas would also favor the effect of photodegradation that converts chemical elements from organic into inorganic form in the marine environment. This process would increase the amount of inorganic carbon of terrestrial origin potentially lowering the CO_2 uptake of the Arctic Ocean [*Bélanger et al.*, 2006]. On the other hand, the effect of enhanced photodegradation could also increase the availability of macronutrients into inorganic form [*Tank et al.*, 2011] with potential positive effects on primary production and hence on the CO_2 uptake of the Arctic Ocean.

[39] Possible changes in the flux of RDOC could be caused by the future warming of regional Arctic climate. In fact, Arctic climate warming could cause the destabilization of the terrestrial organic carbon currently stored in the permafrost pool [*Lawrence et al.*, 2008]. This might lead to an increase in riverine fluxes of organic material [*Frey and McClelland*, 2009] potentially impacting the turbidity of the coastal Arctic waters with implications for vertical penetration of solar radiation, for upper ocean physics, and also for the seasonal cycle of sea-ice. It has been also shown that in the Arctic Ocean the organic matter of terrestrial origin could substantially impact the penetration of irradiance modifying the upper ocean heating rate [*Hill*, 2008], with potential consequences for the water column physical structure and with implications for both ecological and biogeochemical processes. An increase in the concentration of light-absorbing material would increase the heating rate of the upper water column and would accelerate the seasonal melting of sea-ice with cascading effects on ecological and biogeochemical processes in the Arctic Ocean. Some recent work based on models elucidated the role of chlorophyll concentration on upper ocean physics and sea-ice and on the biogeochemical feedbacks related to it [*Manizza et al.*, 2005, 2008]. Nevertheless, there are no studies that quantified the impact of riverine organic material on the physical processes occurring in the upper Arctic Ocean. Models incorporating these processes would help us to predict the response of this complex land-ocean system to future climate warming. Further model-based studies are certainly needed to shed more light on the potential response of the Arctic Ocean, as a biogeochemical system, to the anthropogenic climate change in the near future.

Appendix A: Ocean Biogeochemical Model

[40] In our biogeochemical model used for this study, the temporal evolution of each generic biogeochemical tracer (C) is governed by advection (first term on the right-hand-side), eddy diffusion (second term), and all biogeochemical processes that we define as SMS (source minus sink; third term), as follows:

$$\frac{\partial C}{\partial t} = -u \cdot \nabla C + \nabla \cdot K \nabla C + SMS. \tag{A1}$$

We model the carbon and phosphorus cycles, using a simplified parameterization of export production in which biological uptake and regeneration are indexed to phosphorus. We carry six tracers in the model, phosphate (PO_4), dissolved organic phosphorus (*DOP*), dissolved inorganic carbon (*DIC*), alkalinity, oxygen (O_2, not discussed here), and RDOC. Biological productivity can be limited by the availability of PO_4 or light (I) and is parameterized similar to *McKinley et al.* [2004] and *Parekh et al.* [2005]. The net community productivity is

$$B = \alpha \frac{I}{I + K_I} \frac{PO_4}{PO_4 + K_{PO_4}}, \tag{A2}$$

where $\alpha = 0.5$ μM P month^{-1} is maximum community production, and the half-saturation constants are $K_I = 30$ W m^{-2}, $K_{PO_4} = 0.5$ μM. A large fraction, $\nu = 0.67$, of this primary production enters the *DOP* pool, which has an e-folding timescale for remineralization of 6 months [*Yamanaka and Tajika*, 1996] as adopted for other studies. The remaining fraction of this productivity is instantaneously exported as particulate to depth [*Yamanaka and Tajika*, 1997] where it is remineralized according to the empirical power law relationship determined by *Martin et al.* [1987]. The fate of carbon is linked to that of phosphorus by the Redfield ratio, $R_{C:P}$ (117:1). We will refer, in our results, to "export production", which will be the component of the net community production which is lost to depth: $(1 - \nu)B$. Carbonate chemistry is explicitly solved [*Follows et al.*, 2006] and the air-sea exchange of CO_2 is parameterized with a uniform gas transfer coefficient following *Wanninkhof* [1992].

Appendix B: Tracers Initialization

[41] In order to generate three-dimensional fields of DIC and ALK to initialize our biogeochemical model, we used empirical relationships where DIC and ALK are function of potential temperature and salinity. The values of DIC and ALK were approximated using using simple linear regression models and data from the CARINA Arctic data product [*Key et al.*, 2010; *Jutterström et al.*, 2010]. The parameterizations used temperature and salinity as fitting variables for the upper ocean where the concentrations vary with depth. The deep ocean concentrations were set to constant values as implied by the limited data for both DIC and ALK. Since our study focuses on upper ocean processes, small changes in the deep ocean carbon chemistry will not significantly impact our results. We then used the potential temperature and salinity calculated from our model in 1992 to generate the corresponding three-dimensional fields of DIC and ALK to initialize our model. For depths less than 500 meter, we apply the following equations to derive the DIC and ALK values for model initialization:

$$DIC = (a_1 \cdot \theta) + (b_1 \cdot S) + c_1, \tag{B1}$$

$$ALK = (a_2 \cdot \theta) + (b_2 \cdot S) + c_2, \tag{B2}$$

where θ is the potential temperature (°C), as S is salinity (PSU), $a_1 = -7.46$, $b_1 = 9.41$ $c_1 = 784.4$ μmol kg^{-1}, $a_2 = -1.18$, $b_2 = 44.51$, $c_2 = 752.8$ μmol kg^{-1}. The units for a, b and c are μmol kg^{-1} °C^{-1}, μmol kg^{-1} PSU^{-1}, and μmol kg^{-1}, respectively. For depths greater than 500 m we assign to DIC and ALK constant values of 2158.1 and 2297.3 μmol

kg^{-1}, respectively. We then used the potential temperature and salinity calculated from our model in 1992 to generate the corresponding three-dimensional fields of DIC and ALK to initialize our model by using the equations shown above.

[42] **Acknowledgments.** This study has been carried out as part of ECCO2 and SASS (Synthesis of the Arctic System Science) projects funded by NASA and NSF, respectively. MM and MJF are grateful for support from the National Science Foundation (ARC-0531119 and ARC-0806229) for financial support. MM also acknowledges NASA for providing computer time, the use of the computing facilities at NAS center and also the Scripps post-doctoral program for further financial support that helped to complete the manuscript. RMK also acknowledges NOAA for support (NA08OAR4310820 and NA08OAR4320752). Oliver Jahn kindly provided interpolated phosphate fields for model initialization and Stuart Goldberg nicely helped us with the plots of the CARINA data set by using Ocean Data View.

References

Adcroft, A., C. Hill, and J. Marshall (1997), Representation of topography by shaved cells in a height coordinate ocean model, *Mon. Weather Rev.*, *125*(9), 2293–2315.

Amon, R. M. W., and B. Meon (2004), The biogeochemistry of dissolved organic matter and nutrients in two large Arctic estuaries and potential implications for our understanding of the Arctic Ocean system, *Mar. Chem.*, *92*, 311–330.

Anderson, L. G., S. Jutterström, S. Hjalmarsson, I. Wahlström, and I. P. Semiletov (2009), Out-gassing of CO_2 from Siberian Shelf seas by terrestrial organic matter decomposition, *Geophys. Res. Lett.*, *36*, L20601, doi:10.1029/2009GL040046.

Arakawa, A., and V. Lamb (1977), Computational design of the basic dynamical processes of the UCLA general circulation model, *Methods Comput. Phys.*, *17*, 174–267.

Arrigo, K., G. van Dijken, and S. Pabi (2008), Impact of shriking Arctic ice cover on marine primary production, *Geophys. Res. Lett.*, *35*, L19603, doi:10.1029/2008GL035028.

Bates, N. R. (2006), Air-sea CO_2 fluxes and the continental shelf pump of the carbon in the Chucki Sea adjacent to the Arctic Ocean, *J. Geophys. Res.*, *111*, C10013, doi:10.1029/2005JC003083.

Bates, N. R., and J. T. Mathis (2009), The Arctic Ocean marine carbon cycle: Evaluation of air-sea CO_2 exchanges, ocean acidification impacts and potential feedbacks, *Biogeosciences*, *6*(11), 2433–2459, doi:10.5194/bg-6-2433-2009.

Bates, N. R., S. D. Moran, D. A. Hansell, and J. T. Mathis (2006), An increasing CO_2 sink in the Arctic Ocean due to the sea-ice loss, *Geophys. Res. Lett.*, *33*, L23609, doi:10.1029/2006GL027028.

Batjes, N. H. (1997), Total carbon and nitrogen in the soils of the world, *Eur. J. Soil Sci.*, *47*, 151–163.

Bélanger, S., H. Xie, N. Kroktov, P. Larouche, W. F. Vincent, and M. Babin (2006), Photomineraliztion of terrigenous dissolved organic matter in Arctic coastal waters from 1979 to 2003: Interannual variability and implications of climate change, *Global Biogeochem. Cycles*, *20*, GB4005, doi:10.1029/2006GB002708.

Benner, R., P. Lochouarn, and R. M. W. Amon (2005), Terrigenous dissolved organic matter in the Arctic Ocean and its transport to surface and deep waters of the North Atlantic, *Global Biogeochem. Cycles*, *19*, GB2025, doi:10.1029/2004GB002398.

Condron, A., P. Winsor, C. N. Hill, and D. Menemenlis (2009), Response of Arctic freshwater budget to extreme NAO forcing, *J. Clim.*, *22*, 2422–2437.

Conkright, M. E., H. E. Garcia, T. D. O'Brien, R. A. Locarnini, T. P. Boyer, C. Stephens, and J. I. Antonov (2002), *World Ocean Atlas 2001*, vol. 4, *Nutrients, NOAA Atlas NESDIS*, vol. 52, NOAA, Silver Spring, Md.

Cooper, L. W., R. Benner, J. W. McClelland, B. J. Peterson, R. M. Holmes, P. A. Raymond, D. A. Hansell, J. M. Grebmeier, and L. Codispoti (2005), Linkages among runoff, dissolved organic carbon, and the stable oxygen isotope composition of seawater mass indicators in the Arctic Ocean, *J. Geophys. Res.*, *110*, G02013, doi:10.1029/2005JG000031.

Dutkiewicz, S., A. Sokolov, J. Scott, and P. Stone (2002), A three-dimensional ocean-sea ice-carbon cycle model and its coupling to a two-dimensional atmospheric model: Uses in climate change studies, *Tech. Rep. 122*, Mass. Inst. of Technol. Jt. Program on the Sci. and Policy of Global Change, Cambridge, Mass.

Falck, E., and L. G. Anderson (2005), The dynamics of the carbon cycle in the surface water of the Norwegian Sea, *Mar. Chem.*, *94*, 43–53.

Follows, M. J., S. Dutkiewicz, and T. Ito (2006), On the solution of the carbonate system in ocean biogeochemistry models, *Ocean Modell.*, *12*, 290–301.

Fransson, A., M. Chierici, and Y. Nojiri (2002), New insights into the spatial variability of the surface water carbon dioxide in varying sea ice conditions in the Arctic Ocean, *J. Oceanogr.*, *58*(2), 379–387.

Frey, K. E., and J. W. McClelland (2009), Impact of permafrost degradation on arctic river biogeochemistry, *Hydrol. Processes*, *23*, 169–182.

Hansell, D. A., D. Kadko, and N. R. Bates (2004), Degradation of terrigenous dissolved organic carbon in the western Arctic Ocean, *Science*, *304*, 858–861.

Hibler, W. D., III (1979), A dynamic thermodynamic sea ice model, *J. Phys. Oceanogr.*, *9*, 815–846.

Hibler, W. D., III, and K. Bryan (1987), A diagnostic ice-ocean model, *J. Phys. Oceanogr.*, *17*(7), 987–1015.

Hill, V. J. (2008), Impact of chromophoric dissolved organic material on surface heating of the Chukchi Sea, *J. Geophys. Res.*, *113*, C07024, doi:10.1029/2007JC004119.

Jakobsson, M., R. Macnab, L. Mayer, R. Anderson, M. Edwards, J. Hatzky, H. W. Schenke, and P. Johnson (2008), An improved bathymetric portrayal of the Arctic Ocean: Implications for ocean modeling and geological, geophysical and oceanographic analyses, *Geophys. Res. Lett.*, *35*, L07602, doi:10.1029/2008GL033520.

Jutterström, S., L. G. Anderson, N. R. Bates, R. Bellerby, T. Johannessen, E. P. Jones, R. M. Key, X. Lin, A. Olsen, and A. M. Omar (2010), Arctic Ocean data in CARINA, *Earth Syst. Sci. Data*, *2*, 71–78.

Kalnay, E., et al. (1996), The NCEP/NCAR 40-year reanalysis project, *Bull. Am. Meteorol. Soc.*, *77*, 437–471.

Kattsov, V., and E. Kallen (2005), Future climate change: Modeling and scenarios for the Arctic, in *Arctic Cliamte Impact Assessment*, chap. 4, pp. 99–150, Cambridge Univ. Press, Cambridge, Mass.

Key, R. M., T. Tanhua, A. Olsen, M. Hoppema, S. Jutterström, C. Schirnick, S. V. Heuven, X. Lin, D. Wallace, and L. Mintrop (2010), The CARINA data synthesis project: Introduction and overview, *Earth Syst. Sci. Data*, *2*(1), 579–624.

Lammers, R. B., A. I. Shiklomanov, C. J. Vörösmarty, B. M. Fekete, and B. J. Peterson (2001), Assessment of contemporary Arctic river runoff based on observational discharge records, *J. Geophys. Res.*, *106*(D4), 3321–3334.

Lawrence, D. M. A., A. G. Slater, R. A. Thomas, M. Holland, and C. Deser (2008), Accelerated Arctic land warming and permafrost degradation during rapid sea ice loss, *Geophys. Res. Lett.*, *35*, L11506, doi:10.1029/2008GL033985.

Le Quéré, C., et al. (2005), Ecosystem dynamics based on plankton functional types for global ocean biogeochemistry models, *Global Change Biology*, *11*, 2016–2040, doi:10.1111/j.1365-2486.2005.01004.x.

Macdonald, R. W., L. G. Anderson, J. P. Christensen, L. A. Miller, I. P. Semiletov, and R. Stein (1993), The Arctic Ocean, in *Carbon and Nutrient Fluxes in Continental Margins: A Global Synthesis*, pp. 291–303, Springer, Berlin.

Manabe, S., R. T. Wetherald, P. C. D. Milly, T. L. Delworth, and R. J. Stouffer (2004), Century-scale change in water availability: CO_2 quadrupling experiment, *Clim. Change*, *64*, 59–76.

Manizza, M., C. Le Quéré, A. J. Watson, and E. T. Buitenhuis (2005), Bio-optical feedbacks among phytoplankton, upper ocean physics and sea-ice in a global model, *Geophys. Res. Lett.*, *32*, L05603, doi:10.1029/2004GL020778.

Manizza, M., C. Le Quéré, A. J. Watson, and E. T. Buitenhuis (2008), Ocean biogeochemical response to the phytoplankton-light feedback in a global model, *J. Geophys. Res.*, *113*, C10010, doi:10.1029/2007JC004478.

Manizza, M., M. J. Follows, S. Dutckiewicz, J. W. McClelland, D. Menemenlis, C. N. Hill, A. Townsend-Small, and B. J. Peterson (2009), Modeling transport and fate of riverine dissolved organic carbon in the Arctic Ocean, *Global Biogeochem. Cycles*, *23*, GB4006, doi:10.1029/2008GB003396.

Marshall, J., C. Hill, L. Perelman, and A. Adcroft (1997), Hydrostatic, quasi-hydrostatic and nonhydrostatic ocean modeling, *J. Geophys. Res.*, *102*(C3), 5733–5752.

Martin, J. H., G. Knauer, D. Karl, and W. Broenkow (1987), VERTEX: Carbon cycling in the northeast Pacific, *Deep-Sea Res.*, *34*, 267–285.

McClelland, J. W., et al. (2008), Development of a Pan-Arctic database for river chemistry, *Eos Trans. AGU*, *89*(24), 217–218.

McGuire, A. D., L. G. Anderson, T. R. Christensen, S. Dallimore, L. Guo, D. J. H. M. Heimann, T. D. Lorenson, R. W. Macdonald, and N. Roulet (2009), Sensitivity of the carbon cycle in the Arctic to climate change, *Ecol. Appl.*, *79*(4), 523–555.

McGuire, A. D., et al. (2010), An analysis the carbon cycle of the Arctic Basin form 1997 to 2006, *Tellus B*, *62*, 455–474, doi:10.1111/j.1600-0889.2010.00497.x.

McKinley, G., M. J. Follows, and J. C. Marshall (2004), Mechanisms of air-sea CO_2 flux variability in the Equatorial Pacific and in the North Atlantic, *Global Biogeochem. Cycles*, *18*, GB2011, doi:10.1029/2003GB002179.

McLaughlin, F. A., E. C. Carmack, R. W. MacDonald, and J. K. Bishop (1996), Physical and geochemical properties across the Atlantic/Pacific water mass front in the southern Canadian Basin, *J. Geophys. Res.*, *101*, 1183–1197.

Menemenlis, D., et al. (2005), NASA supercomputer improves prospects for ocean climate research, *Eos Trans. AGU*, *86*(9), 89–96.

Miller, L. A., et al. (2002), Carbon distributions and fluxes in the North Water, 1998 and 1999, *Deep-Sea Res. Part II*, *49*, 5151–5170.

Mucci, A., B. Lansard, L. A. Miller, and T. N. Papakyriakou (2010), CO_2 fluxes across the air-sea interface in the southeastern Beaufort Sea: Ice-free period, *J. Geophys. Res.*, *115*, C04003, doi:10.1029/2009JC005330.

Murata, A., and T. Takizawa (2003), Summertime CO_2 sink in shelf and slope waters of the western Arctic Ocean, *Cont. Shelf Res.*, *23*, 753–776.

Nakaoka, S., S. Aoki, T. Nakazawa, G. Hashida, S. Morinoto, T. Yamanouchi, and H. Yoshikawa-Inoue (2006), Temporal and spatial variations in oceanic pCO_2 and air-sea CO_2 flux in the Greenland Sea and Barents Sea, *Tellus B*, *58*(2), 148–161.

Olsson, K., and L. G. Anderson (1997), Input and biogeochemical transformation of dissolved carbon in the Siberian shelf seas, *Cont. Shelf Res.*, *17*(7), 819–833.

Omar, A. M., T. Johannessen, A. Olsen, S. Katlin, and F. Rey (2007), Seasonal and interannual variabilty of the air-sea CO_2 flux in the Atlantic sector of the Barents Sea, *Mar. Chem.*, *104*, 203–213.

Pabi, S., G. L. van Dijken, and K. Arrigo (2008), Primary production in the Arctic Ocean, 1998–2006, *J. Geophys. Res.*, *113*, C08005, doi:10.1029/2007JC004578.

Parekh, P., M. J. Follows, and E. A. Boyle (2005), Decoupling of iron and phosphate in the global ocean, *Global Biogeochem. Cycles*, *19*, GB2020, doi:10.1029/2004GB002280.

Peterson, B. J., R. M. Holmes, J. W. McClelland, C. J. Vörösmarty, R. B. Lammers, A. I. Shiklomanov, I. A. Shiklomanov, and S. Rahmstorf (2002), Increasing river discharge to the Arctic Ocean, *Science*, *298*, 2171–2173, doi:10.1126/science.1077445.

Ping, C.-L., G. J. Michaelson, L. Guo, M. T. Jorgenson, M. Kanevskiy, Y. Shur, F. Dou, and J. Liang (2011), Soil carbon and material fluxes across the eroding Alaska Beaufort Sea coastline, *J. Geophys. Res.*, *116*, G02004, doi:10.1029/2010JG001588.

Pipko, I. I., I. P. Semiletov, P. Y. Tishchenko, S. P. Pugach, and J. P. Christensen (2002), Carbonate chemistry dynamics in Bering Strait and Chukchi Sea, *Prog. Oceanogr.*, *55*, 77–94.

Raymond, P. A., J. W. McClelland, R. M. Holmes, A. V. Zhulidov, K. Mull, B. J. Peterson, R. G. Striegl, G. R. Aiken, and T. Y. Gurtovaya (2007), Flux and age of dissolved organic carbon exported to the Arctic Ocean: A carbon isotopic study of the five largest arctic rivers, *Global Biogeochem. Cycles*, *21*, GB4011, doi:10.1029/2007GB002934.

Semiletov, I. P. (1999), Aquatic sources of CO_2 and CH_4 in the polar regions, *J. Atmos. Sci.*, *56*(2), 286–306.

Shiklomanov, I., A. Shiklomanov, R. Lammers, B. Peterson, and C. Vorosmarty (2000), The dynamics of river water inflow to the Arctic Ocean, in *The Freshwater Budget of the Arctic Ocean*, edited by E. Lewis, pp. 281–296, Kluwer Acad., Dordrecht, Netherlands.

Skjelvan, I., et al. (2005), A review of the Inorganic Carbon Cycle of the Nordic Seas and Barents Sea, in *The Nordic Seas: An Integrated Perspective Oceanography, Climatology, Biogeochemistry, and Modeling*, *Geophys. Monogr. Ser.*, vol. 158, edited by H. Drange et al., pp. 157–175, AGU, Washington, D. C.

Steele, M., R. Morley, and W. Ermold (2001), PHC: A global ocean hydrography with a high quality Arctic Ocean, *J. Clim.*, *14*, 2079–2087, doi:10.1175/1520-0442(2001).

Steele, M., J. Morison, W. Ermold, I. Rigor, M. Otrmeyer, and K. Shimada (2004), Circulation of summer Pacifc halocline water in the Arctic Ocean, *J. Geophys. Res.*, *109*, C02027, doi:10.1029/2003JC002009.

Steele, M., W. Ermold, and J. Zhang (2008), Artcic Ocean surface warming trends over the past 100 years, *Geophys. Res. Lett.*, *35*, L02614, doi:10.1029/2007GL031651.

Stein, R., and R. W. MacDonald (2003), Organic carbon budget: Arctic Ocean vs. global ocean, in *The Organic Carbon Cycle in the Arctic Ocean*, edited by R. Stein and R. W. Macdonald, chap. 8, pp. 315–322, Springer, Berlin.

Tank, S. E., M. Manizza, J. W. McClelland, R. M. Holmes, and B. J. Peterson (2011), The processing and impact of dissolved riverine nitrogen in the Arctic Ocean, *Estuaries Coasts*, doi:10.1007/s12237-011-9417-3, in press.

Walsh, J. J. (1989), Arctic carbon sinks, *Global Biogeochem. Cycles*, *3*(4), 393–411.

Wanninkhof, R. (1992), Relationship between wind speed and gas exchange over the ocean, *J. Geophys. Res.*, *97*, 7373–7382.

Yamanaka, Y., and E. Tajika (1996), The role of vertical fluxes of particulate organic matter and calcite in the oceanic carbon cycle: Studies using an ocean biogeochemical general circulation model, *Global Biogeochem. Cycles*, *10*(2), 361–382.

Yamanaka, Y., and E. Tajika (1997), The role of dissolved organic matter in the marine biogeochemical cycle: Studies using an ocean biogeochemical general circulation model, *Global Biogeochem. Cycles*, *10*, 599–612.

Zhang, J., and W. D. Hibler III (1997), On an efficient numerical method for modeling sea ice dynamics, *J. Geophys. Res.*, *102*, 8691–8702.

Zhang, J., and D. Rothrock (2003), Modeling global sea ice with a thickness and enthalpy distribution model in generalized curvilinear coordinates, *Mon. Weather Rev.*, *131*(5), 845–861, doi:10.1175/1520-0493(2003)131<0845:MGSIWA>2.0.CO;2.

S. Dutkiewicz, M. J. Follows, and C. N. Hill, Department of Earth, Atmospheric and Planetary Sciences, Massachusetts Institute of Technology, 77 Massachussets Ave., Cambridge, MA 01239, USA.

R. M. Key, Department of Geosciences, Princeton University, Sayre Hall, Princeton, NJ 08544, USA.

M. Manizza, Geosciences Research Division, Scripps Institution of Oceanography, University of California, San Diego, 9500 Gilman Dr., La Jolla, CA 92093-0244, USA. (mmanizza@ucsd.edu)

J. W. McClelland, Marine Science Institute, University of Texas at Austin, 750 Channel View Dr., Port Aransas, TX 78373-5015, USA.

D. Menemenlis, Jet Propulsion Laboratory, California Institute of Technology, Mail Stop 300-323, 4800 Oak Grove Dr., Pasadena, CA 91109-8099, USA.

B. J. Peterson, Ecosystems Center, Marine Biological Laboratory, 7 MBL St., Woods Hole, MA 02543-1015, USA.